The ferroelectric phase transition in pure and lightly doped barium titanate

1991 J. Phys.: Condens. Matter 3 4555

(http://iopscience.iop.org/0953-8984/3/25/005)

J. Phys.: Condens. Matter 3 (1991) 4555–4567. Printed in the UK

The ferroelectric phase transition in pure and lightly doped barium titanate

C N W Darlington† and R J Cernik‡

† School of Physics and Space Research, University of Birmingham, Birmingham B15 2TT, UK

‡ Daresbury Laboratory, Warrington WA4 4AD, UK

Received 23 January 1991, in final form 3 March 1991

Abstract. The effect of light doping on the phase transition to the ferroelectric state in $BaTiO_3$ has been studied using synchrotron radiation at Daresbury Laboratory, UK. Our results indicate that the presence of dilute impurities, which turn $BaTiO_3$ from a wide band-gap intrinsic semiconductor into an extrinsic n-type semiconductor, changes the transition from a discontinuous to a continuous one, and produces large spatial variation in magnitude of the electric polarization in both the high- and low-temperature phases; these fluctuations were barely detectable in the pure, annealed material.

1. Introduction

Pure $BaTiO_3$ undergoes a discontinuous transition to a ferroelectric form at 130 °C (T_t). The transition has been described using soft-mode theory [1], with the transverse optic mode at the zone centre heavily overdamped [2]. Evidence accumulated over the years suggests that there is a cross-over to an order–disorder regime a little above the transition temperature [3–7]. Treating the transition as purely displacive seems inadequate [5, 7].

The experiments described in [3] and [4] used flux-grown crystals and these are known to contain impurities. The EPR experiment described in [5] used a crystal that had been deliberately doped with iron. No details concerning the crystal used in [6] are given. It is more than likely that none of the experiments cited above probed the behaviour of chemically pure $BaTiO_3$. Katib *et al* [7] describe calculations determining the effect of anharmonic interactions on phonon dispersion.

The presence of impurities can radically change the behaviour of many systems; for example, pure $KTaO_3$ does not undergo any phase change down to 0 K, while the introduction of niobium to form $KTa_{1-x}Nb_xO_3$, leads to a 'gradual dipolar clustering process induced by relaxing Nb ions in the $KTaO_3$ lattice' [8] (and references therein).

Studies of the effect of doping on the discontinuous transition in $KMnF_3$ in which the unit cell doubles in each cubic direction [9–11] show that above a certain threshold concentration, in this case between 1 and 10 mole percent of $KMgF_3$, the transition becomes continuous. An analysis of the wavevector dependence of the critical x-ray scattering at the zone boundary above the transition temperature [10] found an exceptionally narrow component in addition to a broader part produced by softening phonons. A central peak was detected in the neutron scattering [11], whose energy width was less

0953-8984/91/254555 + 13 $03.50

than the resolution of the experiment (0.1 THz). Both the narrow component in the x-ray scattering and the central peak seem to be related to random fields in the system, but they have different temperature dependences. Introducing impurities did not significantly increase the intensity of the central peak in the neutron scattering; surprisingly they reduced the intensity of the anomalous narrow component in the x-ray scattering.

We have performed x-ray scattering experiments on powders of pure and lightly-doped $BaTiO_3$ using the facilities at SRS Daresbury. The doped samples had formulae $(Ba_{0.999}Ce_{0.001})TiO_3$, $(Ba_{0.997}Ce_{0.003})TiO_3$ and $Ba(Ti_{0.997}Nb_{0.003})O_3$. These, and the unannealed pure material, gave diffraction patterns markedly different from the pure annealed sample. The effect of both dopants is to change $BaTiO_3$ from a wide band-gap intrinsic semiconductor (~3 eV) to an extrinsic n-type semiconductor, achieved by replacing Ba^{2+} or Ti^{4+} with an ion of higher valency. Experiments are in progress studying the effect on the transition at 130 °C of introducing impurities with the same charge as the ions they replace.

Strain couples electrostrictively to polarization in $BaTiO_3$, so a study of line profiles can give information on both magnitude and spatial variation of the primary order parameter. If the polarization is taken to lie along [001], then

$$\varepsilon_{11} = \varepsilon_{22} = Q_{12}P_3^2 \qquad \varepsilon_{33} = Q_{11}P_3^2$$

leading to a change in Bragg angle given by

$$\Delta(2\theta) = -K[\varepsilon_{11}(h^2 + k^2) + \varepsilon_{33}l^2]$$

where

$$K = [\lambda^2/\{a^2 \sin(2\theta)\}].$$

In $BaTiO_3$, Q_{11} is almost exactly equal to $-2Q_{12}$ [12], so that the unit cell volume is not changed by the onset of polarization.

Studies of the electrical properties of lightly-doped $BaTiO_3$ [13, 14] show an exceptionally large drop in resistivity as the sample enters the ferroelectric state from the cubic phase. In [15] this was attributed to the resistance of blocking layers at surfaces and grain boundaries being reduced by the onset of ferroelectricity.

2. Experimental set-up

2.1. Sample preparation

The doped powders were produced by ball-milling 'puratronic' $BaTiO_3$, obtained from Johnson Matthey Chemicals, Royston, UK, with the relevant quantity of either CeO_2 or Nb_2O_5 under acetone for 30 minutes and then maintaining the mixture at 1200 °C in air for 30 hours held in a platinum-lined crucible. The annealed, pure sample was given the same heat treatment.

Particle size broadening would only contribute to the width of a powder diffraction line if there were a significant fraction of the sample with dimensions less than about 3 μm. In none of the samples was there greater than 1% by weight of particles with mean dimension less than 3 μm. In the pure material, both annealed and unannealed, the volume mean diameter was about 25 μm, while in the doped samples, which had been ball-milled, the volume mean diameter was around 12 μm.

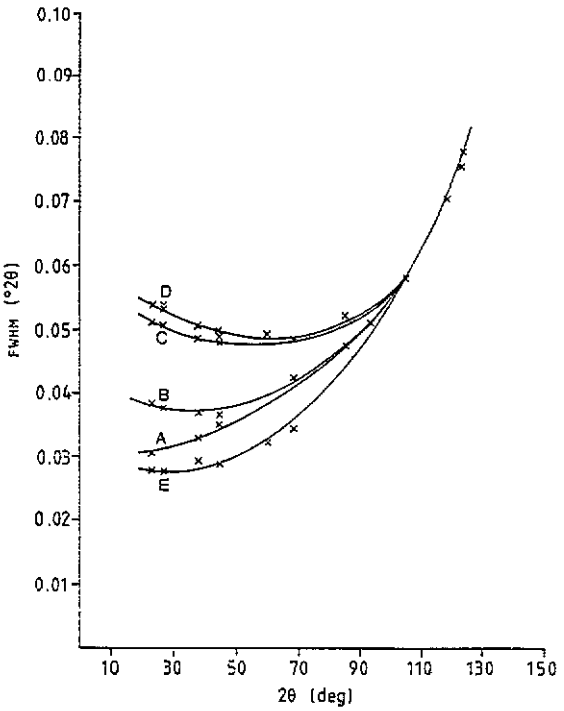

Figure 1. Dependence of FWHM of BaF_2 versus 2θ for various slit configurations. At high Bragg angles, the width is dominated by angular dispersion.

2.2. Diffractometer

The diffractometer on station 9.1 was used in high-resolution mode with simple slit geometry. The sample was mounted in a rotating flat plate specimen holder rather than a capillary because of high absorption by the sample. The experiments were performed on three separate visits to the synchrotron; the wavelength chosen each time was 1 Å since this is close to the critical wavelength on this beam line.

The effects of different slit widths on the instrumental resolution function have been studied recently [16]. The relevant results from a study of a standard sample of BaF_2 are shown in figure 1. Curves A, B and C show the effect of keeping the entrance slit width and angular aperture of the receiving slit constant (5 mm and 0.026° respectively), and changing the entrance slit height as follows: A, 0.2 mm; B, 0.4 mm; C, 0.65 mm. Curve E shows the effect of reducing the receiving slit aperture to 0.018° and the entrance slit height to 0.1 mm, although for most purposes the flux with this slit configuration is unacceptibly low. Curve D was measured with the same conditions as curve C except the entrance slit width was 10 mm; this shows clearly the effects of axial divergence. The choice of slit widths and receiving apertures affects the instrumental resolution function up to approximately 100° in 2θ where the effects of angular dispersion start to dominate the instrumental resolution function.

All the reflections from doped and pure samples in the current study were measured below this angle. Therefore the slits were chosen so that the instrumental resolution function was relatively flat whilst still maintaining an angular resolution of about 0.05° in 2θ.

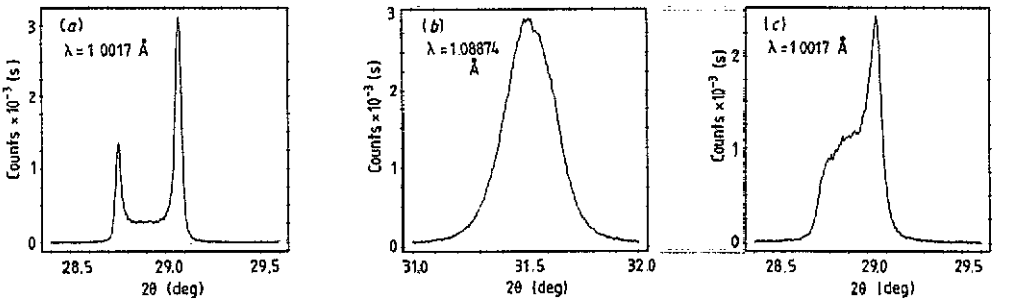

Figure 2. Profiles of (200) near room temperature: (*a*) pure annealed $BaTiO_3$ at 25 °C, (*b*) pure unannealed $BaTiO_3$ at 25 °C, (*c*) $(Ba_{0.997}Ce_{0.003})\,TiO_3$ at 10 °C.

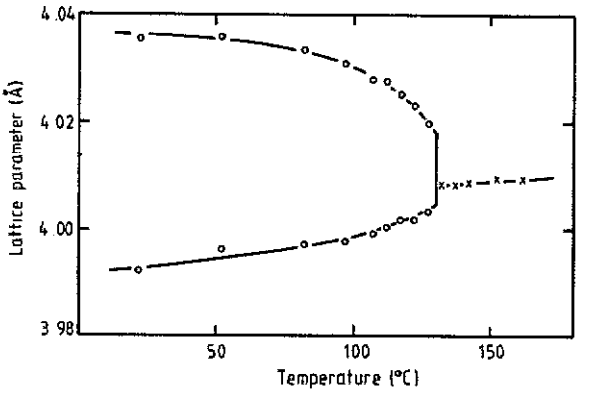

Figure 3. Temperature dependence of lattice parameters for pure annealed $BaTiO_3$.

The sample was mounted in a furnace manufactured by GTP Engineering Ltd. The temperature was maintained by a Newtronic three-term controller, giving a temperature stability of better than 1 °C for all runs. The furnace allows the sample to rotate, and the sample chamber can be filled with different gases, although for this study the sample was surrounded by air.

3. Experimental results

θ–2θ scans through reflections (110), (111), (200), (211) and (220) were made at a number of temperatures for all the samples. The step length was 0.006° in 2θ, and counts were accumulated for 2s at each point. Figure 2 shows the room temperature scans through (200) reflection for the pure annealed sample (figure 2(*a*)), the pure unannealed sample (figure 2(*b*)) and the sample with composition $(Ba_{0.997}Ce_{0.003})\,TiO_3$ (figure 2(*c*)). The other two lightly-doped materials showed similar broadening to that shown in figure 2(*c*).

The temperature dependence of the lattice parameters of the pure annealed sample, obtained from the positions of the two peaks of (200), is shown in figure 3; the discontinuous change occurred at 130 ± 1 °C on heating and 4 °C lower on cooling.

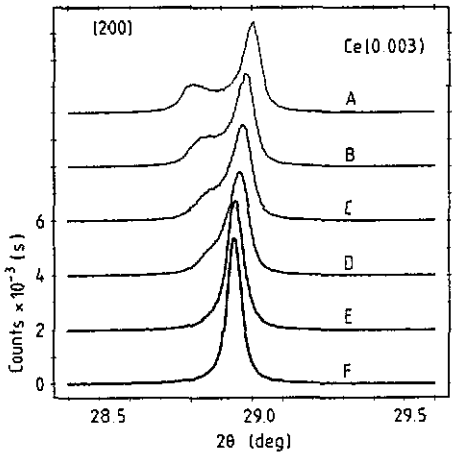

Figure 4. Changes in lineshape of (200) from $(Ba_{0.997}Ce_{0.003})TiO_3$ with temperature. The curve labels denote the following temperatures: A, 85 °C; B, 105 °C; C, 110 °C; D, 115 °C; E, 120 °C; F, 125 °C.

The lineshape of (200) from $(Ba_{0.997}Ce_{0.003})\,TiO_3$ at several temperatures is shown in figure 4. No discontinuous change in c/a is apparent; none could be detected in any of the doped samples, nor in the pure unannealed material.

In the high-temperature phase, the FWHM were dependent on temperature for all samples except the pure annealed one for which the widths were equal to the resolution of the instrument. These findings are discussed in greater detail in the following section.

4. Analysis and discussion

4.1. Pure samples

The slit configuration used for both the annealed and unannealed pure samples resulted in the instrumental resolution being nearly constant over the angular range covered, equal to about 0.047° in 2θ—curve C of figure 1. (During each of the three visits, the resolution function was checked by measuring FWHM of reflections from the pure, annealed sample at temperatures above T_t).

4.1.1. Annealed sample. If the tetragonal distortion were uniform and $(c/a - 1)$ about 0.01 at room temperature, then one would have expected the profiles shown in figure 2 to be asymmetric doublets with the peaks separated.

The profile shown in figure 2(a) is made up of two sharp peaks with FWHM equal to the resolution of the instrument with additional scattering between them. This scattering shows that there is a reduced value of c/a in approximately 20% of the sample. A similar profile was obtained with neutrons on this sample using HRPD at ISIS, Rutherford–Appleton Laboratory [17].

In the ferroelectric phase 90° domain walls will cause microstrain in addition to dislocations, point defects etc. FWHM obtained for temperatures above T_t for the pure annealed sample are given in table 1 and these are equal to the resolution of the instrument i.e. at elevated temperature no line broadening from any source could be detected. This suggests that the additional intensity between the peaks at room temperature is due to scattering from material forming 90° domain walls.

Table 1. Temperature dependence of FWHM × 10^4 (°2θ) of reflections from the pure annealed material in the cubic phase.

	hkl				
T/°C	(110)	(111)	(200)	(211)	(220)
132	492(3)	470(2)	484(3)	467(2)	454(2)
145	490(2)	468(2)	468(2)	462(2)	456(2)
175	481(2)	473(3)	473(2)	467(2)	450(2)

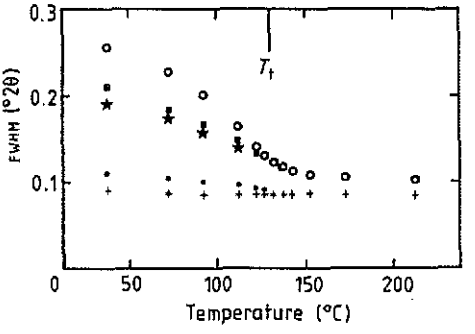

Figure 5. Temperature dependence of FWHM of several reflections from pure unannealed $BaTiO_3$. T_t, shown on the figure, is the transition temperature for the pure annealed material. Above T_t, the widths of (110) and (111) are virtually the same, as are the widths of (200), (211) and (220). The symbols denote: ●, (110); +, (111); ○, (200); ★, (211); ■, (220).

Within these walls the structure must be severely distorted, with the electric polarization on one side of the wall nearly perpendicular to its direction on the other. Additional intensity would occur between the peaks if the magnitude of the polarization varied in a 'tanh-like' fashion through the wall.

These walls produce a change in the overall shape of a crystal, hence their presence can partially relieve stress. An estimate of their thickness from direct optical observation [18] gave a value of about 1000 unit cells or 0.4 μm.

4.1.2. Unannealed sample. The broadened profile (in figure 2(*b*)) from the pure unannealed sample indicates that a much greater portion of the sample has reduced value of c/a ratio resulting in a nearly symmetric peak. Figure 5 shows the temperature dependence of FWHM of several reflections from this sample. These values were obtained by fitting a single asymmetric pseudo-Voigt function to the profiles. There is a change of sign in the curvature of these plots at the same temperature as the discontinuous change in the pure annealed material. The profiles obtained at room temperature after this run was completed were indistinguishable from the profiles measured before the temperature was raised; in fact the points at 90 and 70 °C were measured on cooling from 210 °C.

As the temperature is decreased from 210 °C, the widths increase, apart from that for the reflection (111), with the magnitude of the increase depending on (*hkl*), indicating that the structure possesses an anisotropic distortion. An estimate of this was obtained by subtracting the experimental widths at 210 °C from values measured at lower temperatures. At 210 °C the lines have a Lorentzian component of typically 80%. From the expression for $\Delta(2\theta)$ given in the introduction one can calculate the difference in Bragg angle for the two components making up each doublet. These are compared with the

Table 2. Values, in arbitrary units, of calculated splitting of reflections and estimates of the experimentally determined anisotropic broadening.

First column, Miller indices; second column, calculated splitting; third column, FWHM from pure unannealed sample at room temperature; fourth column, FWHM from $(Ba_{0.999}Ce_{0.001})TiO_3$ measured at its transition temperature; fifth column, FWHM from $(Ba_{0.997}Ce_{0.003})$ TiO_3 measured at its transition temperature; sixth column, FWHM from $Ba(Ti_{0.997}Nb_{0.003})O_3$ measured at its transition temperature.

hkl	$\Delta(2\theta)$	PUSRT	Ce(0.001)	Ce(0.003)	Nb(0.003)
111	0	3	0	−3	4
110	35	15	33	50	36
211	63	62	50	67	51
220	74	75	68	100	66
200	100	100	100	100	100

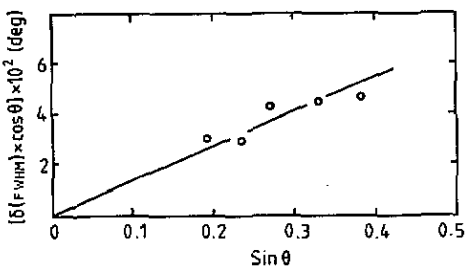

Figure 6. Williamson–Hall plot of (excess FWHM) × $\cos(\theta)$ versus $\sin(\theta)$ for pure unannealed $BaTiO_3$ measured at 210 °C.

(scaled) experimental estimates of the anisotropic broadening in table 2, having taken $Q_{11} = -2Q_{12}$. Clearly the anisotropy in the linewidths is the result of a tetragonal distortion of the structure, which increases as the temperature falls, and is consistent with $Q_{11} = -2Q_{12}$.

The transition in the unannealed material is smeared out with parts of the sample possessing pseudotetragonal symmetry above 130 °C. Subtracting 0.047 °C from the experimentally determined FWHM at 210 °C produces a Williamson–Hall plot (figure 6), which shows that there is considerable, nearly isotropic, strain broadening. The intercept on the ordinate is inversely proportional to the particle size while the slope is proportional to the broadening due to strain—the line drawn was constrained to go through the origin. The microstrain, defined as $\Delta d/d$, is about 1×10^{-3}, which is exceptionally large. It is well established that such straight-forward analysis can lead to significant errors [19], however the result will not be out by more than a factor of two.

The cause of this nearly isotropic strain is unknown, but since it can be removed by annealing it is likely to be either line or point defects and not impurities. For example, the unannealed sample may be deficient in oxygen. Much of the sample would contain symmetry-breaking defects, and hence local displacements would persist in the 'cubic' phase. There would be clusters of polarized material in the high-temperature phase, smearing out the transition and causing broadening of lines as observed. However, if the sample were deficient in oxygen one might have expected the transition temperature to be different from 130 °C.

Table 3. Transition temperatures (T_t) and the temperature below which fluctuations in polarization can be detected (T_d), both measured in °C.

	T_t	T_d
$BaTiO_3$	130	
$(Ba_{0.999}Ce_{0.001})TiO_3$	127	155
$(Ba_{0.997}Ce_{0.003})TiO_3$	122	155
$Ba(Ti_{0.997}Nb_{0.003})O_3$	120	165

4.2. Lightly doped samples

The slit configuration used for the lightly doped samples was different from that used for the pure samples. The height of the entrance slit was reduced to 0.4 mm in order to decrease the component of instrumental broadening. The angular resolution was better, producing lines more nearly Lorentzian in shape—the weight of the Lorentzian component was greater than 0.8—but the FWHM was more dependent on Bragg angle as shown in figure 1, curve B.

The changes in lineshape with temperature for one of the samples is shown in figure 4. Within the resolution of the experiment the transition is continuous and occurs at a well defined temperature with no hysteresis; the other two doped samples showed exactly the same behaviour with slightly different transition temperatures.

The transition temperatures were determined from fitting a single, symmetric pseudo-Voigt function to the profiles. The lowest temperature at which the difference plot was featureless, i.e. gave no evidence of any asymmetry, was taken to be the transition temperature: see table 3. Impurities lower the transition temperature, with the results in broad agreement with those reported in [14]. In the high-temperature phase, all reflections examined were symmetric, indicating that the overall symmetry is cubic.

Figure 7 shows the temperature dependence of the FWHM of reflections in the high-temperature phase. These diverge as $(T - T_t)$ decreases. As the lines are essentially Lorentzian at all temperatures above T_t, the widths can be taken to be the sum of two Lorentzian components; one due to instrumental and non-critical sample broadening, the other describing the critical behaviour. As described earlier, a good estimate of the critical broadening can be obtained by subtracting the linewidths at elevated temperature from the widths obtained at lower temperatures. These (scaled) differences are given in table 2 for the three doped samples at temperatures just above T_t and show that the diverging component is caused by a developing tetragonal distortion, and for this reason can be associated with the presence of spatial variation in polarization.

The magnitude of the divergence is similar in the samples with 0.3 mol.% doping, and about three times less in the sample doped with 0.1 mol.% impurity.

The temperature dependence of this excess width has been fitted using the expression

$$\delta(2\theta) = W(T - T_s)^{-s}$$

where W, T_s and s are constants. T_s was determined by varying its value to make the plot of $\log[\delta(2\theta)]$ versus $\log[T - T_s]$ linear. For all three doped samples T_s was close to 112 °C—see figure 8—and hence appears to be determined by the host crystal and not the impurity or its concentration. Figure 9 shows plots of $\log[\delta(2\theta)]$ versus $\log[T - T_s]$. Both cerium-doped samples have a value of s of about 2.75 while the niobium-doped

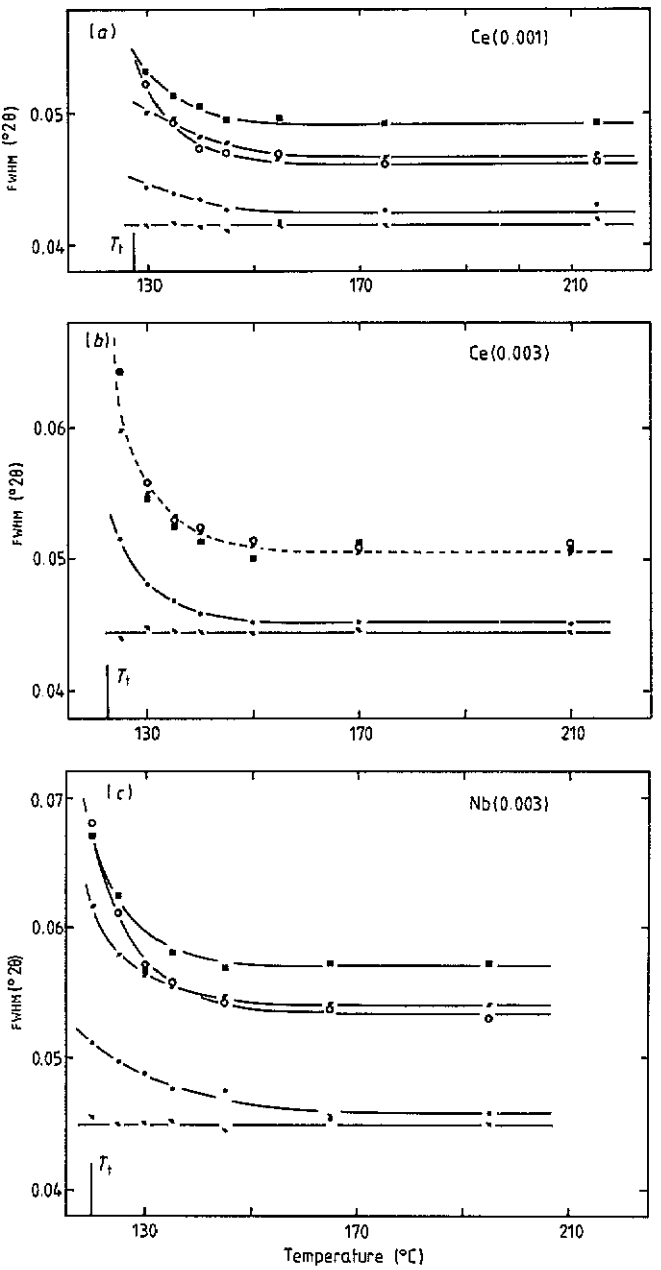

Figure 7. Temperature dependence of FWHM of several reflections from the doped samples above their transition temperatures. The symbols denote: ●, (110); ◥, (111); ○, (200); ◩, (211); ■, (220).

sample has a value of 1.6. A value of 1.3 was obtained for the pure unannealed material. The error in each exponent is ±0.2.

The reciprocal dielectric susceptibility in the high-temperature phase of nominally pure $BaTiO_3$ extrapolates to zero at a temperature T_c which is about 13 °C less than the

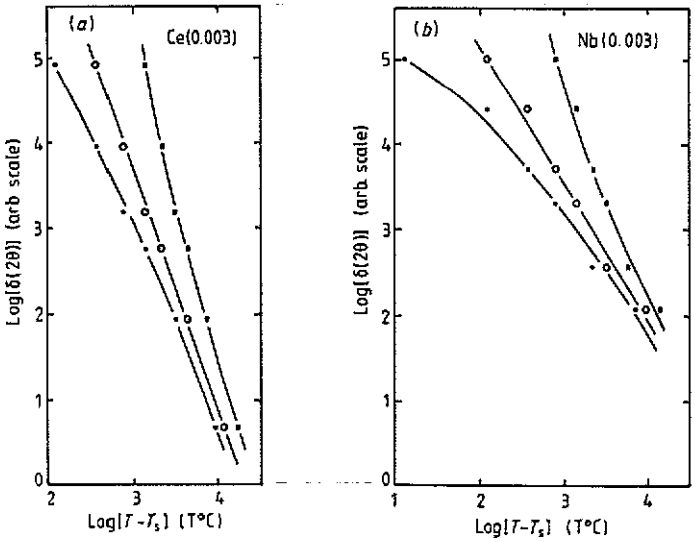

Figure 8. Effect of choice of T_s on the plot of $\log[\delta(2\theta)]$ versus $\log[T - T_s]$ for the (200) reflection. The symbols denote the following temperatures: ■, T_s = 102 °C; ○, T_s = 112 °C; ●, T_s = 117 °C.

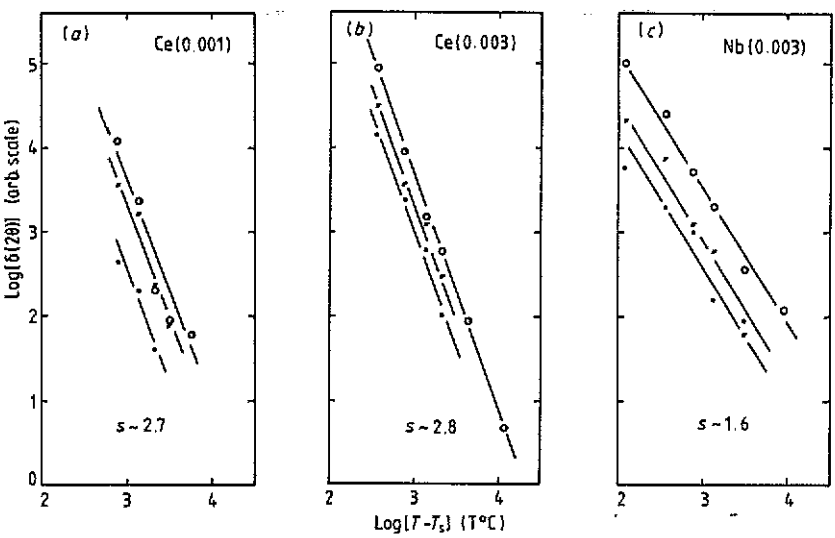

Figure 9. $\text{Log}[\delta(2\theta)]$ versus $\log[T - T_s]$ for the three doped samples with T_s set equal to 112 °C. The same symbols have been used as in figure 7. (220) has been omitted for the sake of clarity.

temperature at which the discontinuous change to the ferroelectric form occurs [20], so it is tempting to identify T_s with T_c.

Clearly, although the transitions in the doped samples appear continuous, they differ from continuous transitions in pure materials in which the transition occurs at T_c.

The behaviour of the doped samples should depend not only on the charge of the dopant but on whether the impurities are symmetry conserving or symmetry breaking

[21]. A symmetry-conserving impurity occupies a site of high symmetry, either substitutionally or interstitially, while a symmetry-breaking impurity occupies a site that lowers the symmetry. However, this classification is incomplete, since the impurity may hop rapidly enough between symmetry-related symmetry-breaking sites, so that on the timescale of the experiment the defect becomes symmetry conserving. For an x-ray scattering experiment this latter complication is not relevant.

At sufficiently high temperatures no broadening of the lines is observed, and so, at least at these temperatures, the impurities do not change the local symmetry.

Symmetry-conserving defects may favour the formation of the low-temperature phase or stabilize the high-temperature phase. In the former case there exists a temperature (T_d), not well defined but greater than T_t, below which the low-temperature structure begins to form around defect sites. As temperature is decreased below T_d, the size of these clusters grows as the correlation length of the host crystal increases. Whether the transition temperature in the doped material is above or below T_t of the pure material is not clear, since the existence of regions of local order may act to inhibit phonon softening, thereby lowering the temperature at which the correlation length reaches a critical value [21].

From figure 7 values of T_d can be identified, and are given in table 3.

If symmetry-conserving defects stabilize the high-temperature phase, then the local static susceptibility is reduced below that of the pure material, and locally the transition temperature will be lowered. It is hard to see why fluctuations in the high-temperature phase should be enhanced by defects of this kind.

Symmetry-breaking defects give rise to Huang scattering. As discussed in [22], this scattering would be expected to be linearly dependent on concentration of the impurity and, at a reciprocal lattice point, i.e. $q = 0$, diverge as $(t)^{-2\gamma}$, where t is the reduced temperature and γ the exponent of the susceptibility of the host crystal; the q-dependence would be Lorentzian. In our case the impurities are charged and the soft mode has zero wavevector which complicates the analysis, and may alter the behaviour of the scattering close to T_t [22].

From a macroscopic viewpoint, the fluctuation–dissipation theorem relates susceptibility to fluctuations in polarization to give

$$k_B T \chi_T = V_c[\langle P^2 \rangle - \langle P \rangle^2] \tag{1}$$

where V_c is the volume within which the fluctuations are correlated, and presumably should equal the cube of the correlation length. However, the experiments described in [3] which measured the refractive index in the high-temperature phase of nominally pure $BaTiO_3$ found that the correlation volume was only weakly temperature dependent, and approximately equal to 5×10^4 Å^3 i.e. about 800 unit cells.

Using values for the electrostrictive coefficients and Curie constant, C, given in [12] for pure $BaTiO_3$ and assuming that

$$\chi_T = C(T - T_s)^{-s}$$

then V_c for both cerium-doped samples is about 10^3 Å^3, and about 5×10^4 Å^3 for the niobium-doped sample; from the temperature dependence assumed for χ_T, V_c will be independent of temperature.

The effect of the doping used here makes $BaTiO_3$ an n-type extrinsic semiconductor. In chapter 14 of [23], it has been pointed out that there will be the following two important consequences.

(i) Mobile carriers reduce the susceptibility and the (quartic) anharmonicity. Both effects lower the transition temperature in systems which are ferroelectric in the intrinsic semiconducting state.

(ii) Ion–electron correlations lead to a screening of the Coulombic ion–ion interaction, thereby reducing its range and increasing the temperature interval $|T - T_t|$ within which the behaviour of the system is fluctuation dominated.

Lowering of T_t and fluctuations in order parameter have been observed caused either by soft, symmetry-conserving defects, or mobile charge carriers, or possibly both.

5. Conclusions

The effects of light doping on the behaviour of $BaTiO_3$ can be summarized as follows:

(1) The values of T_t—the temperatures at which the overall symmetry changes, i.e. the transition temperatures—and T_c (T_s) in the doped samples are different. Therefore, even though the transitions appear continuous, they are different from continuous transition in pure materials in which the transition occurs at T_c.

(2) There is a well defined temperature (measured to within ±2 °C) at which the overall symmetry changes. This is lower than the transition temperature in the pure material.

(3) Spatial variation in polarization is greatly enhanced in both phases.

(4) If the defects are symmetry conserving then they are soft, i.e. they favour the formation of the low-temperature phase at temperatures above T_t of the pure sample. Alternatively, if they break the local symmetry, then the observed broadening of the lines should follow the temperature dependence of the static susceptibility of the host crystal. One would have anticipated that the values of exponent s would have been the same for the cerium-doped and niobium-doped samples. Since this is not the case, then it is more likely that the defects conserve symmetry.

Acknowledgments

We wish to thank SERC for funding this research.

References

[1] Cochran W 1960 *Adv. Phys.* **9** 387
[2] Harada J, Axe J D and Shirane G 1971 *Phys. Rev.* B **4** 155
[3] Cohen M G, DiDomenico M Jr and Wemple S H 1970 *Phys. Rev.* B **1** 4334
[4] Comès R, Lambert M and Guinier A 1968 *Solid State Commun.* **6** 715
[5] Müller K A and Berlinger W 1986 *Phys. Rev.* B **34** 6130
[6] Müller K A, Luspin Y, Servoin J L and Gervais F 1982 *J. Physique* **43** L537
[7] Katib D, Migoni R, Kugel G E and Godefroy L 1989 *J. Phys.: Condens. Matter* **1** 9811
[8] Fontana M D, Bouziane E and Kugel G E 1990 *J. Phys.: Condens. Matter* **2** 8681
[9] Cox U J, Gibaud A and Cowley R A 1988 *Phys. Rev. Lett.* **61** 982
[10] Cox U J 1989 *J. Phys.: Condens. Matter* **1** 3565
[11] Cox U J and Cussen L D 1989 *J. Phys.: Condens. Matter* **1** 3579
[12] Jona F and Shirane G 1962 *Ferroelectric Crystals* (Oxford: Pergamon)

[13] Harman G G 1957 *Phys. Rev.* **106** 1358
[14] Saburi O 1959 *J. Phys. Soc. Japan* **14** 1159
[15] Heywang W 1971 *J. Mater. Sci.* **6** 1214
[16] Langford J I, Cernik R J and Louer D 1990 *J. Appl. Crystallogr.* at press
[17] Darlington C N W and David W I F 1990 unpublished
[18] Little E A 1955 *Phys. Rev.* **98** 978
[19] Langford J I, Delhez R, de Keijser Th H and Mittemeijer E J 1988 *Aust. J. Phys.* **41** 173
[20] Burfoot J C 1967 *Ferroelectrics: an Introduction to the Physical Principles* (London: van Nostrand)
[21] Halperin B I and Varma C M 1976 *Phys. Rev.* B **14** 4030
[22] Bruce A D and Cowley R A 1981 *Structural Phase Transitions* (London: Taylor and Francis)
[23] Lines M E and Glass A M 1977 *Principles and Applications of Ferroelectrics and Related Materials* (Oxford: Clarendon) ch 14